

# 2.5D Transformer: An Efficient 3D Seismic Interpolation Method without Full 3D Training

Changxin Wei<sup>1</sup>, Xintong Dong<sup>1</sup>, Xinyang Wang<sup>2</sup>

<sup>1</sup> *State Key Laboratory of Deep Earth Exploration and Imaging, College of Instrumentation and Electrical Engineering, Jilin University, Changchun 130026, China. E-mail: [dxt@jlu.edu.cn](mailto:dxt@jlu.edu.cn)*

<sup>2</sup> *College of Electric Engineering, Department of Communication Engineering, Key Laboratory of Modern Power System Simulation and Control and Renewable Energy Technology (Ministry of Education), Northeast Electric Power University, Jilin 132012, China*

22 January 2026

## SUMMARY

Transformer has emerged as a powerful deep-learning technique for two-dimensional (2D) seismic data interpolation, owing to its global modeling ability. However, its core operation introduces heavy computational burden due to the quadratic complexity, hindering its further application to higher-dimensional data. To achieve Transformer-based three-dimensional (3D) seismic interpolation, we propose a 2.5-dimensional Transformer network (T-2.5D) that adopts a cross-dimensional transfer learning (TL) strategy, so as to adapt the 2D Transformer encoders to 3D seismic data. The proposed T-2.5D is mainly composed of 2D Transformer encoders and 3D seismic dimension adapters (SDAs). Each 3D SDA is placed before a Transformer encoder to learn spatial correlation information across seismic lines. The proposed cross-dimensional TL strategy comprises two stages: 2D pre-training and 3D fine-tuning. In the first stage, we optimize the 2D Transformer encoders using a large amount of 2D data patches. In the second stage, we freeze the 2D Transformer encoders and fine-tune the 3D SDAs using limited 3D data volumes. Extensive experiments on multiple datasets are conducted to assess the effectiveness

and efficiency of T-2.5D. Experimental results demonstrate that the proposed method achieves comparable performance to that of full 3D Transformer at a significantly low cost.

**Key words:** Machine Learning, Image processing, Neural networks, fuzzy logic

## 1 INTRODUCTION

Interpolation operation is a crucial step for improving the quality of seismic data, especially when facing geometries with large spatial sampling intervals, and recovering missing parts caused by topographical constraints, limited budgets, or receiver malfunctions. By reconstructing the missing information and compensating the sparse geometries, effective interpolations can enhance the completeness and continuity of events, facilitating the subsequent inversion and high-resolution imaging ([Chen et al. 2024](#); [Cheng et al. 2025](#)).

To acquire the desired dense and complete seismic data, geophysical scholars have proposed various conventional interpolation methods over the past few decades ([Spitz 1991](#); [Trad et al. 2002](#); [Oropeza & Sacchi 2011](#)). These methods are theory-driven, relying on mathematical models or analytical formulations to describe the underlying physical processes. Generally, they can be divided into four categories: the wave-equation-based, prediction filtering, low-rank, and sparse-representation methods.

The wave-equation-based methods utilize subsurface velocity models to simulate the propagation of seismic wavefields, so as to reconstruct the incomplete data ([Wang et al. 2019](#)). [Ronen \(1987\)](#) proposed a trace-interpolation method based on the wave equation and prior assumption of a smooth spatial spectrum, and experimental results have demonstrated its effectiveness on both synthetic and field data. The offset-continuation differential equation-based method proposed by [Fomel \(2003\)](#) showed good interpolation performance even in several structurally complex situations. However, the wave-equation based methods often require a relatively accurate velocity model as an important prerequisite, which is often unavailable in numerous real-world problems. Moreover, the heavy computation burden seriously limits their further applications.

The prediction filtering methods exploit the correlation of events in different domains to perform the interpolation operation. When applying these methods, the interpolation task is taken as a

least-squares linear inverse problem, and interpolated results are generated by minimizing the misfit between the predicted and input data (Liu et al. 2022b). Spitz (1991) proposed a multichannel and model-free interpolation method for missing traces in f-x domain, exhibiting good interpolation performance in both pre- and post-stack examples. To further improve the interpolation performance, Naghizadeh & Sacchi (2007) proposed a multistep autoregressive algorithm-based prediction-error method combined with Fourier-based methods to reconstruct seismic data from low to all frequencies. An important assumption of these prediction filtering methods is that events are required to be linear. However, this is usually not satisfied in real conditions, resulting in serious interpolation performance degradation.

The low-rank methods assume that the complete seismic data in a specific arrangement is of low rank at a given frequency component (Trickett et al. 2010; Gao et al. 2013), and missing traces will significantly increase its rank. Therefore, the interpolation tasks can be accomplished by reducing the rank to an optimal one. Typical low-rank methods include singular spectrum analysis (SSA; Vautard & Ghil 1989; Oropeza & Sacchi 2011; Carozzi & Sacchi 2021), matrix completion (Ma 2013; Yang et al. 2013; Kumar et al. 2015), principal component analysis (Wold et al. 1987; Huang et al. 2016; Wu et al. 2023), and Cadzow filtering (Cadzow 2002; Gao et al. 2013; Naghizadeh & Sacchi 2013; Huang et al. 2020). Oropeza & Sacchi (2011) proposed a simultaneous denoising and reconstruction method for seismic data based on multichannel SSA (MSSA), which resembles seismic data interpolation with the method of projection onto convex sets (POCS). Moreover, a randomized singular value decomposition is adopted to accelerate its rank reduction stage. Ma (2013) enhanced the matrix completion using a designed texture-patch transformation, exhibiting superior performance to traditional POCS method. However, in these low-rank methods, the determination of optimal rank is an intricate problem, and an improper one will have a negative impact on the interpolated results (Ma 2013; Cheng et al. 2023).

The sparse-representation methods interpolate seismic records by representing them into sparse domains. The useful signals and the missing data are treated as large- and small-amplitude coefficients, respectively. Preserving the large-amplitude coefficients and eliminating the small-amplitude ones helps to extract the useful signal components from the incomplete data (Chen et al. 2019).

The missing signal components are then recovered through an inverse sparse transform. These methods can be mainly categorized into mathematical transform-based (Trad et al. 2002; Yu et al. 2007; Fomel & Liu 2010; Naghizadeh & Sacchi 2010) and dictionary learning-based (Liang et al. 2014; Yu et al. 2015; Wang et al. 2020) methods. Trad et al. (2002) proposed a high-resolution time-variant Radon transform (RT)-based interpolation method. Hyperbolic and elliptical RTs are implemented to perform accurate interpolation and attenuate sampling artifacts in poorly sampled common-midpoint gathers. Based on the good sparse representation ability of shearlet transform, Liu et al. (2018) proposed a multi-component crossline seismic data reconstruction method based on sparse shearlet constraint inversion, achieving better results than traditional wavelet, curvelet, and shearlet methods in several extremely sparse sampling cases. However, most of the above mathematical transform-based methods are based on fixed bases (Liang et al. 2014). To learn basis functions adaptively, experts have developed dictionary learning-based interpolation methods. Liang et al. (2014) attempted to restore decimated seismic data using data-driven tight frame (DDTF) first developed by Cai et al. (2014). The DDTF can adaptively learn from the data itself, and provides a sparser representation for the data in turn. Yu et al. (2015) extended the DDTF to high-dimensional versions and achieves the simultaneous denoising and interpolation of 3D and 5D seismic data. Nevertheless, these sparse-representation methods are hampered by inherent limitations, despite their excellent anti-aliasing and interpolation performance. First, the sparsity of data is an essential assumption. Second, the choice of parameters plays a crucial role. For instance, for the curvelet transform, inaccuracies in the estimation of the mask function can directly affect interpolation performance; for the seislet transform, inaccurate estimation of the local event slope tends to deteriorate the fidelity of seismic data reconstruction. (Wang et al. 2019).

Generally, the successful applications of these conventional methods must satisfy a certain number of prior assumptions, including an accurate subsurface velocity model, the linearity of events, the low-rank structures of seismic data, and the sparsity of signals (Jia & Ma 2017; Wang et al. 2019; Dong et al. 2025). However, it is usually difficult to ensure that the understanding of the subsurface structure is consistent with real conditions (Cheng et al. 2024b), restricting the effectiveness and adaptability of these theory-driven interpolation approaches in handling several

real and complex scenarios (Jia & Ma 2017). These theory-driven methods also involve complex and sophisticated operations for parameter adjustments, which extremely requires expert knowledge and hands-on experience. Additionally, the heavy computational cost that occasionally occurs is also a major hurdle, especially when handling with large-scale and high-dimensional seismic datasets (Wang et al. 2019; Dong et al. 2022).

In recent years, deep learning (DL; LeCun et al. 2015) have attracted much attention. This kind of data-driven techniques has the ability to learn from data itself and process large amounts of data more efficiently (Cheng et al. 2024b). These characteristics enable DL-based methods perform well without prior assumptions and handcrafted parameters, so as to automatically process large-scale datasets. At the early stage, convolutional neural networks (CNNs) have been the primary focus. Typical CNN-based architectures, such as U-Net (Ronneberger et al. 2015; Park et al. 2019, 2021; Fang et al. 2021), Res-Net (He et al. 2016; Wang et al. 2018, 2019; Liu et al. 2022a), and generative adversarial network (GAN; Goodfellow et al. 2014; Siahkoohi et al. 2018; Oliveira et al. 2018), have shown great promise for the seismic data interpolation. Various improvements applied to CNNs have also contributed to further enhance the interpolation performance, including the attention-enhanced CNNs (Yu & Wu 2021), depthwise separable CNNs (Jin et al. 2023), and multi-scale CNNs (Cheng et al. 2023; Dong et al. 2024a,b). As researchers have gained deeper insights into DL-based interpolation methods, the local perception has emerged as a major bottleneck of CNNs, which hinders the further enhancement of the interpolation performance using DL. To address this issue, experts have turned to Transformer (Vaswani et al. 2017) owing to its strong ability to extract global contextual information using self-attention mechanism. Cheng et al. (2024a) proposed a seismic interpolation Transformer network, which is an encoder-decoder structure, with Swin-Transformer blocks forming a U-shaped structure between the encoder and decoder. This approach can effectively reconstruct the consecutively missing traces in distributed acoustic sensing-vertical seismic profiling data. By integrating the global and local features, Gao et al. (2024) proposed a Swin-Transformer convolutional residual network for the simultaneous denoising and interpolation of seismic data, gaining better visual performance and quantitative indices than conventional methods and CNN-based methods. A dense double branch attention Trans-

former (D2AT) proposed by [Dong et al. \(2025\)](#) can effectively reconstruct the consecutively missing traces. The core module of D2AT is a global feature unit composed of six Swin-Transformer blocks distributed in two scales, and this method has shown great interpolation performance and generalization in both pre-stack and post-stack datasets.

Although these DL-based methods have achieved superior performance over conventional methods, they primarily focus on two-dimensional (2D) interpolation and overlook the spatial structure correlation that could be exploited in a 3D interpolation workflow ([Wang et al. 2019](#); [Liu et al. 2022a](#); [Dong et al. 2025](#)). However, 3D feature extraction operations usually introduce significantly greater computational burdens for DL-based interpolations. This phenomenon is particularly prominent when applying Transformer-based architectures, whose computational complexity scales quadratically with the size of input data ([Vyas et al. 2020](#)). Moreover, extending 2D networks to 3D versions will significantly increase the number of trainable parameters ([Ye et al. 2019](#)). Several scholars have made attempts on 3D seismic data interpolation based on 3D CNNs in recent years ([Qian et al. 2021](#); [Chen et al. 2023](#); [Saad et al. 2023](#); [Wang et al. 2025](#)), but most of these methods suffer from heavy computational burdens. Obviously, this phenomenon will become more severe in 3D Transformers due to their quadratic computational complexity. To the best of our knowledge, no prior effort has attempted to apply Transformers to 3D seismic data interpolation at this stage, as training a 3D Transformer network on 3D seismic datasets demands prohibitively large computational resources.

A recent study ([Pan et al. 2022](#)) demonstrates a promising approach to address the above challenges. [Pan et al. \(2022\)](#) proposed an image-to-video transfer learning (TL) strategy that can transfer an 2D image model to a 3D video model using parameter-efficient fine-tuning operations. Inspired by this, we propose a lightweight 2.5-dimensional (2.5D) Transformer (T-2.5D) network to reconstruct 3D incomplete seismic data without using a large amount of 3D volumes to optimize a 3D Transformer network. The proposed T-2.5D is a hybrid of 2D and 3D modules, including four 2D Transformer encoders and four 3D seismic dimension adapters (SDAs). We design a 2D-to-3D cross-dimensional TL workflow to optimize the T-2.5D. This workflow contains two stages: a 2D pre-training stage and a 3D fine-tuning stage. In the 2D pre-training stage, we use 2D training

patches to just optimize the four 2D Transformer encoders without SDAs. In the 3D fine-tuning stage, we freeze the trainable parameters of the four 2D Transformer encoders and use limited 3D volumes to train the four 3D SDAs. This fine-tuning stage enables the T-2.5D to learn spatial correlation information of 3D seismic data. Overall, we use the ‘2D pre-training + 3D fine-tuning’ to replace the time-consuming and memory-intensive full 3D training, so as to significantly alleviate the computational cost of 3D Transformer-based interpolation. We investigate the interpolation performance of T-2.5D on several 3D seismic volumes. Experimental results show that the T-2.5D achieves comparable interpolation performance to 3D Transformer at a significantly lower computational cost. In other words, the proposed T-2.5D achieves a better trade-off between interpolation performance and computational cost.

## 2 METHODOLOGIES

In this section, detailed descriptions of the Transformer, Transformers with different dimensions, cross-dimensional TL, and Transformer-based interpolation theory are provided in the following subsections.

### 2.1 Transformer

As a classical DL framework, Transformer has gained significant attention from academia and industry in recent years. It has been applied to the fields of natural language processing (Vaswani et al. 2017) and computer vision (Dosovitskiy 2020). Owing to the core operation, MSA, Transformer is capable of capturing the global contextual information and shows better performance than CNNs in numerous cases.

To prepare a 1D input sequence for the Transformer encoder shown in Fig. 1a, we first flatten the 2D input matrix using positional encoding and shape transformation (i.e., the 2D Handler in Fig. 1a). Then, the flattened feature is input into a layer normalization (LN) layer and an MSA layer, and it is also added to the original input using a residual connection. The output feature of MSA is then fed into another LN layer and a multi-layer perceptron (MLP) layer, and is added to the final output feature via the second residual connection. The output of Transformer encoders is

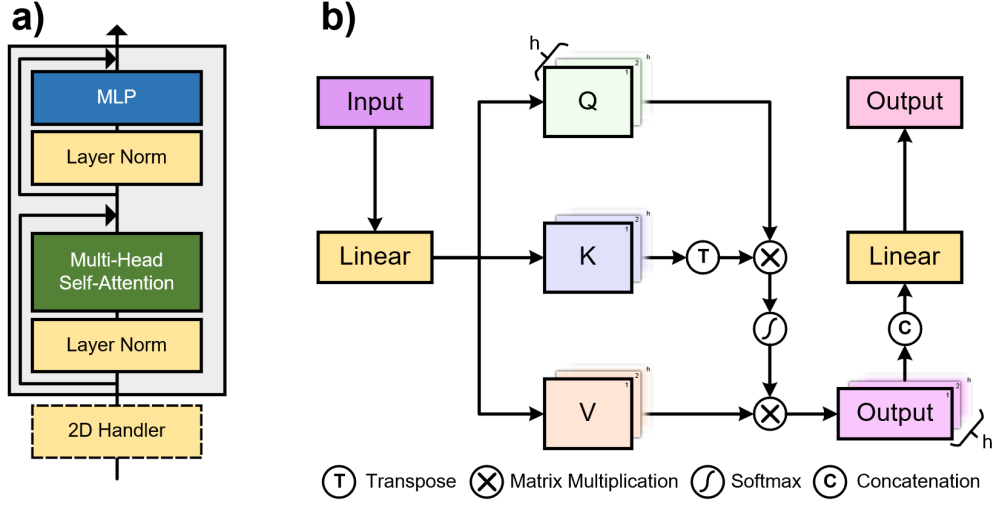


**Figure 1.** Architecture of Transformer. (a) Transformer encoder for 2D features, and (b) calculation process of MSA.

expressed as follows:

$$\mathbf{X}_1 = H2D(\mathbf{X}) \quad (1)$$

$$\mathbf{X}_2 = MSA(LN(\mathbf{X}_1)) + \mathbf{X}_1 \quad (2)$$

$$\mathbf{Y} = MLP(LN(\mathbf{X}_2)) + \mathbf{X}_2 \quad (3)$$

where  $\mathbf{X}$  and  $\mathbf{Y}$  are the input and output features of Transformer encoders, and  $H2D$  represents the 2D handler including the positional encoding and shape transformation. For brevity,  $H2D$  or 3D handler is omitted in subsequent descriptions.

The implementation of MSA is illustrated in Fig. 1b. To compute the self-attention of the  $i$ -th head, the input feature is linearly projected into queries ( $\mathbf{Q}_i$ ), keys ( $\mathbf{K}_i$ ) of channel number  $d_k$ , and values ( $\mathbf{V}_i$ ) of channel number  $d_v$ . First, we transpose the vector  $\mathbf{K}_i$ . Second, after the matrix multiplication between  $\mathbf{Q}_i$  and  $\mathbf{K}_i^T$ , the product is divided by  $\sqrt{d_k}$  and then input into a softmax function to generate the weights for  $\mathbf{V}_i$ . Finally, the attention value is obtained by multiplying  $\mathbf{V}_i$  with its weights. The process is described by the following equation:

$$Attention_i(\mathbf{Q}_i, \mathbf{K}_i, \mathbf{V}_i) = softmax\left(\frac{\mathbf{Q}_i \mathbf{K}_i^T}{\sqrt{d_k}}\right) \mathbf{V}_i. \quad (4)$$

In order to fuse the information from various representation sub-spaces, the single-head attention is expanded to multi-head attention by projecting  $\mathbf{Q}$ s,  $\mathbf{K}$ s and  $\mathbf{V}$ s for  $h$  times using separate learn-

able linear layers. These  $h$  attentions are then integrated using concatenation operation. Finally, a linear projection is utilized to project the channel number back to the same as the input. The MSA is calculated as follows:

$$MSA(\mathbf{Q}, \mathbf{K}, \mathbf{V}) = \text{Linear}(\text{Concat}(A_1, A_2, \dots, A_h)), \quad (5)$$

where  $A_i$  is the abbreviation of  $Attention_i$ .

## 2.2 Transformers with different dimensions

In this paper, we have designed three Transformer-based networks with different dimensions, including a full 2D Transformer (T-2D), a full 3D Transformer (T-3D) and a 2.5D Transformer (T-2.5D). They are highly similar in terms of architecture to ensure clear and relatively fair comparisons. Detailed descriptions of these three networks are provided below.

### 2.2.1 T-2D/3D

In Fig. 2a, the T-2D is composed of three  $3 \times 3$  convolutional layers (Convs), a head block (HB), four 2D Transformer encoders, and a tail block (TB). A 2D patch with a size of  $40 \times 40$  is firstly input into the first Conv, and the channel number is increased from 1 to 32. Then, the features with a size of  $40 \times 40 \times 32$  are input into HB whose structure is shown in Figure 2b. The HB consists of two identical parts, and each one comprises two Convs, a rectified linear unit (ReLU), and a residual connection. The output features of HB are propagated into the core module of T-2D: four successively-connected Transformer encoders, thereby capturing long-range dependencies. Moreover, dense connections [Huang et al. \(2017\)](#), whose effectiveness has been validated by [Dong et al. \(2025\)](#), are deployed to enrich the feature interactions among the four Transformer encoders. Then, a Conv is used to refine the global feature, and an LN layer is deployed to stabilize the training. Subsequently, the TB displayed in Fig. 2c is used for final feature refinement, which is composed of three Convs interleaved with leaky ReLUs in a feed-forward manner. The TB enables efficient non-linear transformation while mitigating the risk of neuron inactivation. The output features of TB and HB are fused via a residual connection, thus avoiding the phenomenon

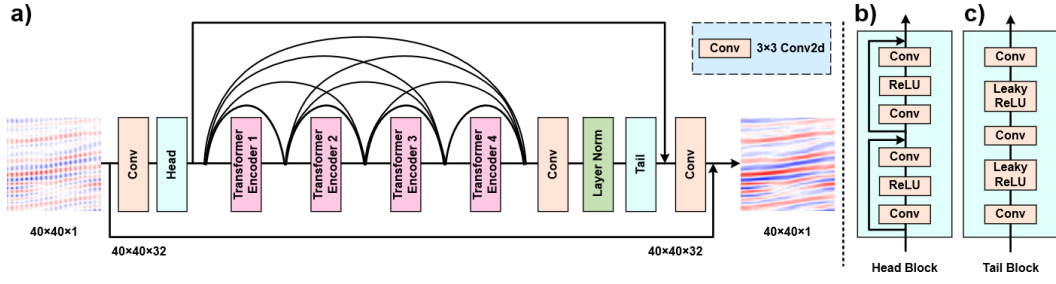


**Figure 2.** Illustration of the T-2D. (a-c) Architectures of T-2D, HB and TB, respectively.

of gradient vanishing. Finally, to generate the final output feature, the last Conv is used to integrate features across channel dimension and reduce the channel number back to one.

We replace all replaceable layers of T-2D with their 3D counterparts to generate the T-3D shown in Fig. 3.

### 2.2.2 T-2.5D

The T-2.5D is generated by adding four 3D SDAs to T-2D. In Fig. 4a, we place a 3D SDA before each 2D Transformer encoder. As shown in Fig. 4b, the 3D SDA is composed of two linear layers and a depth-wise 3D Conv (DWConv3d). Specifically, the first linear layer is used to project the input feature into a 3D space, allowing the following DWConv3d to capture abundant spatial contextual information. Another linear layer is used to project the feature back to the original dimension. A residual connection is utilized to send the input to the output, to prevent potential information loss.

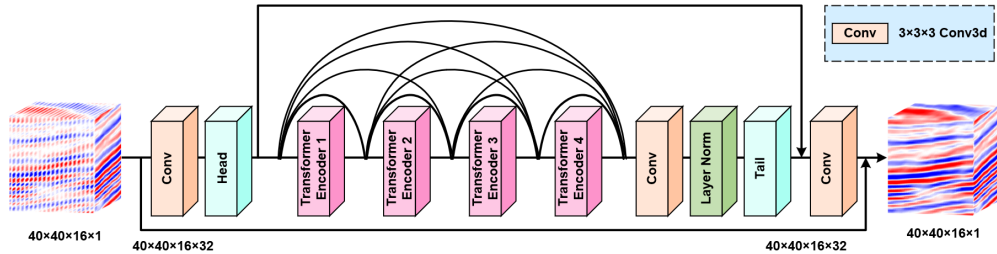


**Figure 3.** Architecture of the T-3D, showing the changes in the dimensions of feature maps from  $40 \times 40$  to  $40 \times 40 \times 16$  and network components from 2D to 3D.

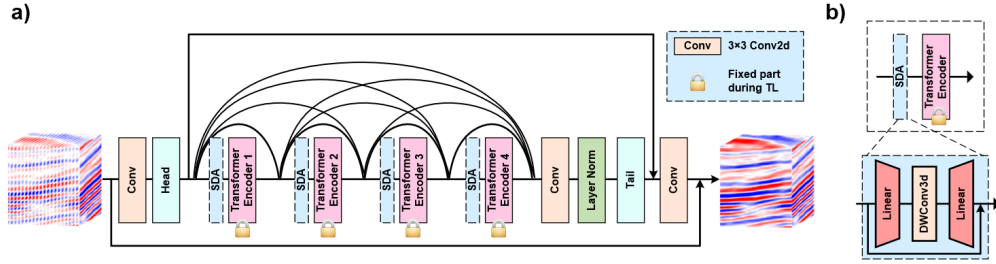


Figure 4. (a) and (b) Architectures of the T-2.5D and SDA, respectively.

### 2.3 Cross-dimensional TL

We utilize a cross-dimensional TL strategy to optimize the T-2.5D. This workflow comprises two stages, including a 2D pre-training one and a 3D fine-tuning one. In the first stage, we optimize the four 2D Transformer encoders of the T-2.5D using a large number of 2D patches, so as to generate a 2D pre-trained model. In the second stage, we freeze the trainable parameters of the four Transformer encoders and use a small amount of 3D volumes to optimize the four 3D SDAs of T-2.5D, where spatial information across seismic lines is learned. The overall process of the cross-dimensional TL is provided in Fig. 5.

### 2.4 Transformer-based Interpolation Theory

#### 2.4.1 2D/3D Interpolation

For the complete 2D seismic data  $x$ , its corresponding incomplete 2D data  $y$  can be expressed as:

$$y = Ax, \tag{6}$$

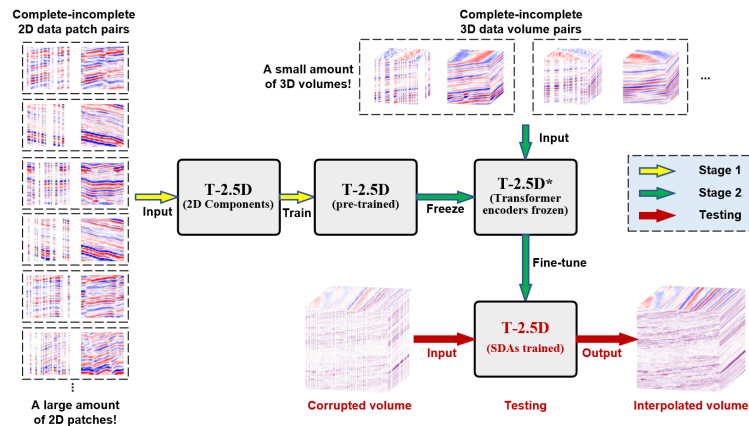


Figure 5. Cross-dimensional TL of the T-2.5D.

where  $\mathbf{A}$  represents a 2D masking matrix used to generate the decimated data with missing traces. Through the network training of T-2D, we can establish a nonlinear mapping relationship  $T_{2D}$  between  $\mathbf{x}$  and  $\mathbf{y}$ , and the trainable parameters of T-2D  $\theta_{2D}$  is updated by minimizing the L<sub>2</sub>-norm loss function in Eq. (7).

$$l(\theta_{2D}) = \frac{1}{B} \sum_{i=1}^B \|T_{2D}(\mathbf{y}_i, \theta_{2D}) - \mathbf{x}_i\|^2, \theta_{2D} = \{\boldsymbol{\omega}, \mathbf{b}\}, \quad (7)$$

where  $\boldsymbol{\omega}$  and  $\mathbf{b}$  denote the weights and biases, respectively,  $B$  is the batch size (i.e., the pair number of training data patches used in one iteration),  $\mathbf{x}_i$  and  $\mathbf{y}_i$  represent the  $i$ -th paired training data patches, and  $\|\cdot\|$  denotes the L<sub>2</sub> norm. In this paper, we use the ADAM algorithm [Kingma & Ba \(2014\)](#) to update the trainable parameters in an iterative manner. Upon obtaining the optimal parameters  $\theta_{2D}^{opt}$ , we can generate the interpolated result  $\hat{\mathbf{x}}_{opt}$  by inputting the incomplete data  $\mathbf{y}$  into the nonlinear relationship  $T_{2D}$ :

$$\hat{\mathbf{x}}_{opt} = T_{2D}(\mathbf{y}, \theta_{2D}^{opt}). \quad (8)$$

The principle of 3D interpolation is similar to the 2D case, where we utilize 3D data to optimize the 3D trainable parameters of T-3D.

#### 2.4.2 2.5D Interpolation

In this paper, we utilize two-stage training strategy to optimize the trainable parameters of T-2.5D,  $\theta_{2.5D}$ , so as to achieve the 2.5D interpolation using Transformer. The  $\theta_{2.5D}$  is composed of  $\theta'_{2D}$ ,  $\theta'_{3D}$ , representing the trainable parameters of the 2D Transformer encoders and 3D SDAs, respectively.

In the 2D pre-training stage, the loss function is updated as follows:

$$l_{stage1}(\theta'_{2D}) = \frac{1}{B} \sum_{i=1}^B \|T_{2.5D}(\mathbf{y}_i^{2D}, \theta'_{2D}) - \mathbf{x}_i^{2D}\|^2, \quad (9)$$

where  $\mathbf{x}_i^{2D}$  and  $\mathbf{y}_i^{2D}$  denote the  $i$ -th paired 2D training data patches, respectively. Upon obtaining the optimal parameters  $\theta'_{2D}^{opt}$ , we freeze them and use a small amount of 3D volumes to optimize the 3D SDAs. In the 3D fine-tuning stage, the loss function is updated through Eq. (10).

$$l_{stage2}(\theta_{2.5D}) = \frac{1}{B} \sum_{i=1}^B \|T_{2.5D}(\mathbf{y}_i^{3D}, \bar{\theta}'_{2D} \cup \theta'_{3D}) - \mathbf{x}_i^{3D}\|^2, \quad (10)$$

where  $\mathbf{x}_i^{3D}$  and  $\mathbf{y}_i^{3D}$  represent the  $i$ -th paired 3D training data volumes, respectively, and  $\bar{\theta}'_{2D}$

**Table 1.** Hyperparameters of T-2D, T-3D, and T-2.5D.

Hyperparameters	Specifications
Optimizer	ADAM
Loss function	L2 norm
Data patch size	40×40 (T-2D), 40×40×16 (T-3D and T-2.5D)
Batch size	1
Number of epochs	20
Learning rate	$10^{-4}$ , $10^{-5}$
Input channel number	1
Embedding channel number	32
Total layers	4

denotes the frozen parameters of 2D Transformer encoders. After certain iterations of the fine-tuning stage, we can obtain a set of optimal 2.5D parameters  $\theta_{2.5D}^{opt}$ . The final 3D interpolation result  $\hat{\mathbf{x}}_{opt}^{3D}$  is generated by inputting the incomplete 3D data  $\mathbf{y}^{3D}$  into the 2.5D nonlinear relationship  $T_{2.5D}$  as follows:

$$\hat{\mathbf{x}}_{opt}^{3D} = T_{2.5D}(\mathbf{y}^{3D}, \theta_{2.5D}^{opt}). \quad (11)$$

The specific process of 2.5D interpolation is given in Algorithm 1.

### 3 EXPERIMENTS

#### 3.1 Training and Hyperparameters Settings

The training program is executed on Pytorch 2.5.1 and CUDA 12.4, running on an Ubuntu 22.04 operation system. Hardware configurations consist of an NVIDIA L20 GPU with 48GB of memory, an Intel Xeon Platinum 8457C CPU with 48 cores at 2.6GHz frequency, and 100GB RAM. Taking into account performance, computational resources, and fair comparison, we set the hyperparameters as shown in Table 1.

**Algorithm 1** 2.5D Interpolation

**Require:**  $T_{2.5D}$ , the nonlinear relationships of 2.5D Transformer;  $B$ , batch size;  $E_1$  and  $E_2$ , the numbers of epochs for the two stages, respectively;  $K$ , the number of iterations in each epoch;  $D_{2D}$  and  $D_{3D}$ , 2D and 3D complete datasets, respectively;  $\mathbf{y}$ , the 3D volume to be tested.

1: **STAGE 1: 2D PRE-TRAINING.**2: **for**  $i=1,2,\dots,E_1$  **do**3:   **for**  $j=1,2,\dots,K$  **do**4:     Sample  $C_{2D} = \{\mathbf{x}_k | k = 1, 2, \dots, B\}$ , a batch of complete data patches, from  $D_{2D}$ .5:     Normalization:  $C_{2D}^n = \{\mathbf{x}_k^n | \mathbf{x}_k^n = \mathbf{x}_k / \max(C_{2D}), k = 1, 2, \dots, B\}$ .6:     Sample  $I_{C_{2D}} = \{\mathbf{y}_k^n | \mathbf{y}_k^n = RM(\mathbf{x}_k^n), \mathbf{x}_k^n \in C_{2D}^n, k = 1, 2, \dots, B\}$ , a batch of incomplete data patches from  $C_{2D}^n$ , where  $RM$  represents the operation of removing traces.7:     Loss iteration:  $\theta'_{2D} \leftarrow \nabla_{\theta} [\frac{1}{B} \sum_{k=1}^B \|T_{2D}(\mathbf{y}_k^n, \theta'_{2D}) - \mathbf{x}_k^n\|^2]$ ,  $\mathbf{x}_k^n \in C_{2D}^n$ ,  $\mathbf{y}_k^n \in I_{C_{2D}}$ .8:     **end for**9:   **end for**10: Optimal parameters obtained:  $\theta_{2D}^{opt}$ .11: **STAGE 2: 3D FINE-TUNING.**12: Get  $\bar{\theta}'_{2D}$ , the frozen  $\theta'_{2D}$ .13: **for**  $i=1,2,\dots,E_2$  **do**14:   **for**  $j=1,2,\dots,K$  **do**15:     Sample  $C_{3D} = \{\mathbf{x}_k | k = 1, 2, \dots, B\}$ , a batch of complete data patches, from  $D_{3D}$ .16:     Normalization:  $C_{3D}^n = \{\mathbf{x}_k^n | \mathbf{x}_k^n = \mathbf{x}_k / \max(C_{3D}), k = 1, 2, \dots, B\}$ .17:     Sample  $I_{C_{3D}} = \{\mathbf{y}_k^n | \mathbf{y}_k^n = RM(\mathbf{x}_k^n), \mathbf{x}_k^n \in C_{3D}^n, k = 1, 2, \dots, B\}$ , a batch of incomplete data volumes from  $C_{3D}^n$ , where  $RM$  represents the operation of removing traces.18:     Loss iteration:  $\theta_{2.5D} \leftarrow \nabla_{\theta} [\frac{1}{B} \sum_{k=1}^B \|T_{2.5D}(\mathbf{y}_k^n, \bar{\theta}'_{2D} \cup \theta'_{3D}) - \mathbf{x}_k^n\|^2]$ ,  $\mathbf{x}_k^n \in C_{3D}^n$ ,  $\mathbf{y}_k^n \in I_{C_{3D}}$ , where  $\theta'_{3D}$  is the trainable parameters of the four SDAs.19:     **end for**20:   **end for**21: Optimal parameters obtained:  $\theta_{2.5D}^{opt}$ .22: **INTERPOLATION.**

### 3.2 Metrics for Interpolation Results

In this study, the peak signal-to-noise ratio (PSNR) and structural similarity index measure (SSIM; Wang et al. 2004) are used to evaluate the performance of different methods quantitatively. The PSNR of 2D data is defined as the following equation:

$$PSNR = 10 \log_{10} \left\{ \frac{[max(\mathbf{x})]^2}{\sum_{i=0}^{M-1} \sum_{j=0}^{N-1} [\mathbf{x}(i, j) - \mathbf{y}(i, j)]^2} \right\}, \quad (12)$$

where  $\mathbf{x}$  and  $\mathbf{y}$  denote the complete and interpolated data, respectively,  $M$  represents the number of sample points in each trace,  $N$  is number of traces, and  $max(\mathbf{x})$  represents the maximum value of  $\mathbf{x}$ . Similarly, the 3D version of PSNR is expressed as follows:

$$PSNR = 10 \log_{10} \left\{ \frac{[max(\mathbf{x})]^2}{\sum_{i=0}^{S-1} \sum_{j=0}^{I-1} \sum_{k=0}^{X-1} [\mathbf{x}(i, j, k) - \mathbf{y}(i, j, k)]^2} \right\}, \quad (13)$$

where  $S$ ,  $I$ , and  $X$  denote the number of sampled points along the time, inline, and crossline axes, respectively.

SSIM is a commonly used metric to evaluate the perceptual similarity between two data. It considers the changes in structural information, luminance, and contrast (Wang et al. 2004). Given a 2D/3D complete data  $\mathbf{x}$  and its corresponding interpolated result  $\mathbf{y}$ , SSIM is defined as:

$$SSIM(\mathbf{x}, \mathbf{y}) = \frac{(2\mu_x\mu_y + C_1)(2\sigma_{xy} + C_2)}{(\mu_x^2 + \mu_y^2 + C_1)(\sigma_x^2 + \sigma_y^2 + C_2)}, \quad (14)$$

where  $\mu_x$  and  $\mu_y$  represent the means of  $\mathbf{x}$  and  $\mathbf{y}$ , respectively,  $\sigma_x^2$  and  $\sigma_y^2$  are the variances of  $\mathbf{x}$  and  $\mathbf{y}$ , respectively,  $\sigma_{xy}$  is the covariance between  $\mathbf{x}$  and  $\mathbf{y}$ , and  $C_1$ ,  $C_2$  are small constants to stabilize the division of whole equation. The value of SSIM ranges from 0 to 1, with higher value indicating greater similarity.

### 3.3 Test of Kerry Dataset

#### 3.3.1 Data preparation and training

We firstly use the Kerry dataset obtained from New Zealand to evaluate the effectiveness and efficiency of T-2.5D. The time sampling interval is 0.004 s. We extract a volume of 256 time samples, 650 inline points, and 186 crossline points from the Kerry dataset as shown in Fig. 6a. The training and test blocks are defined by red and green double arrows in Fig. 6a, respectively. In

T-2D, we extract 7500 2D slices with a shape of  $40 \times 40$  from the training block, and split them into training and validation sets in a ratio of 4:1. Similarly, in T-3D, 7500 3D volumes ( $40 \times 40 \times 16$ ) are extracted from the training block and partitioned into training and validation sets with the same 4:1 ratio. In the first stage of T-2.5D, we pre-train the 2D Transformer encoders using the same dataset as in T-2D. The second stage of T-2.5D utilizes 2000 and 500 3D volumes as training and validation sets, respectively, to fine-tune the 3D SDAs. We randomly remove 40%–60% of the traces in each complete data patch/volume to generate complete-incomplete data pairs. Fig. 6b–6g displays the L2 loss curves for both training and validation of the three methods. After training, we input the test data into the three trained models to evaluate the interpolation performance. Notably, the interpolated result of T-2D is generated by processing the test data line by line and reassembling the outputs into a 3D volume.

### 3.3.2 Testing results

As shown in Fig. 7a, the test data is of shape  $224 \times 224 \times 20$  extracted from Fig. 6a. We randomly delete 50% of the traces to generate the incomplete data in Fig. 7e. Fig. 7b–7d presents the reconstruction results. Fig. 7f–7h display the residual images between the interpolated results (Fig. 7b–7d) and the complete data (Fig. 7a), and Fig. 7i–7k are the local similarity (Fomel 2007) maps between Fig. 7f–7h and Fig. 7a. Both of them are utilized to measure the signal leakage of the interpolated results, and lower energy indicates better interpolation performance. We can observe that all the three methods are able to reconstruct the missing traces to some extent. However, T-2D exhibits stronger signal leakage than T-3D and T-2.5D as shown in Fig. 7f and 7i. In comparison, T-2.5D achieves a comparable performance to T-3D, which validates the effectiveness of T-2.5D.

For a clearer comparison, the sixth line is plotted in 2D (Fig. 8). Due to the lack of spatial correlation information, T-2D yields the poorest performance. This is evidenced by its significantly lower quantitative results and the most severe signal leakage among all networks, as shown in Fig. 8b and 8f. In comparison, T-2.5D achieves an interpolation result close to that of T-3D, and both of their residual images show visually little signal leakage.

Furthermore, we plot in Fig. 9 the f-k spectra of the complete data (Fig. 8a), 50% randomly

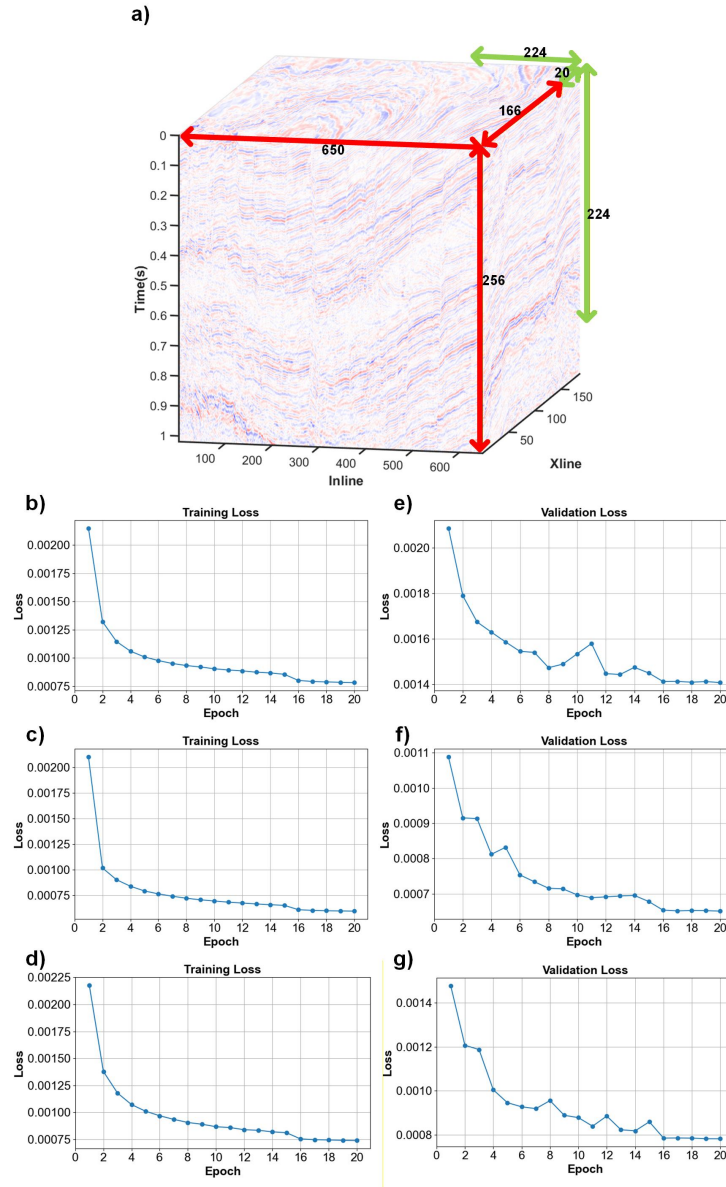


**Figure 6.** (a) 3D Volume of the Kerry dataset, (b–d) training loss curves of T-2D, T-3D and T-2.5D, respectively; and (e–g) the corresponding validation loss curves.

sampled data (Fig. 8e), the three interpolated results (Fig. 8b–8d), and the corresponding residual images (Fig. 8f–8h). As illustrated in Fig. 9b–9d, the aliased energy presented in corrupted data (Fig. 9e) has been largely removed by all the three methods. However, as shown in Fig. 9f, stronger residual interference exists in the result of T-2D. It is also observed in Fig. 9h that the energy leakage of T-2.5D is evidently weaker than that of T-2D, and is very close to that of T-3D.

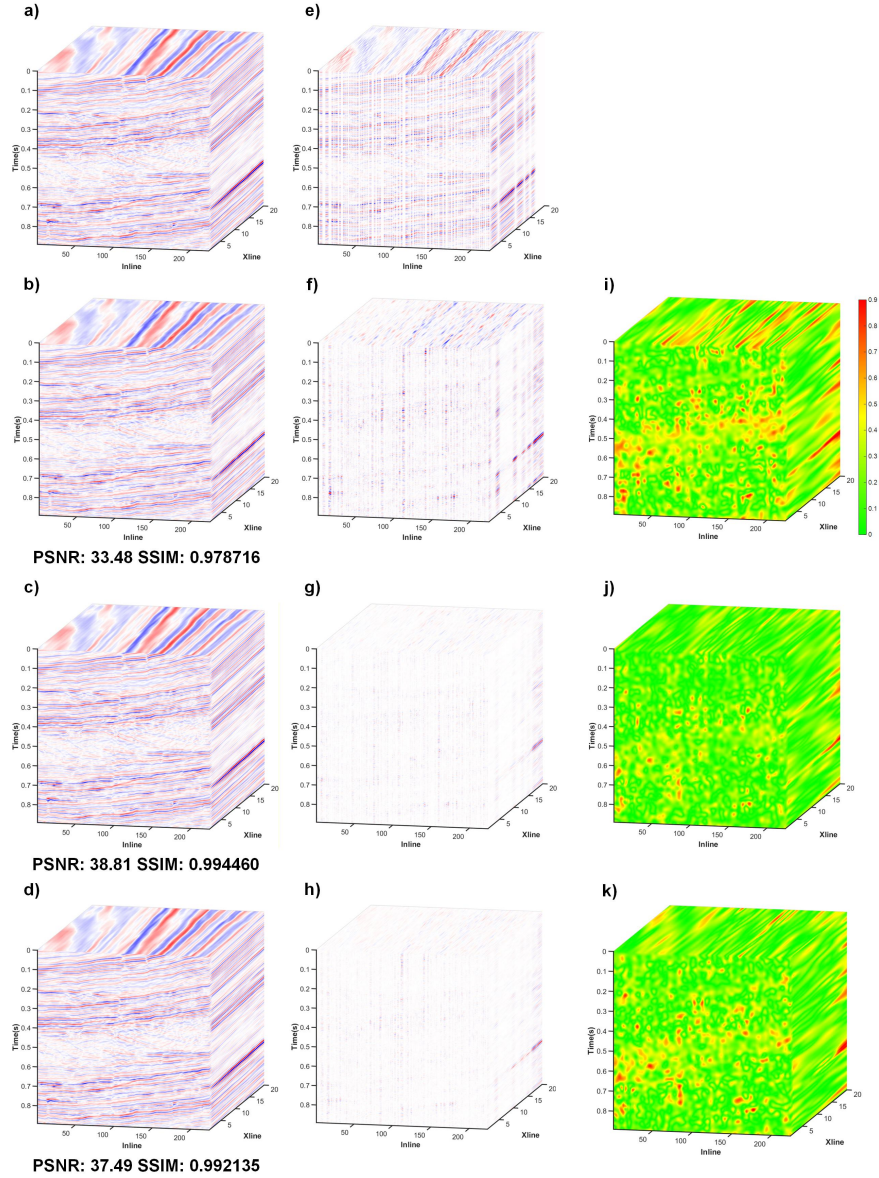


**Figure 7.** Interpolation results of Kerry dataset. (a) Complete data, (e) 50% randomly sampled data, (b–d) interpolated results of T-2D, T-3D and T-2.5D, respectively; (f–h) the corresponding residual images, and (i–k) local similarity maps between (f–h) and (a).

### 3.3.3 Analysis of the computational cost

Computational cost plays a crucial role in DL-based methods as it directly reflects the efficiency of different methods. We have recorded the peak memory usage and training time of the three networks in Table 2. Notably, the total training time of T-2.5D is composed of the pre-training time of the first stage and the training time of the second stage. T-2.5D requires only about 1/12 the memory of T-3D with the training time reduced to approximately 1/20. Generally, T-2.5D

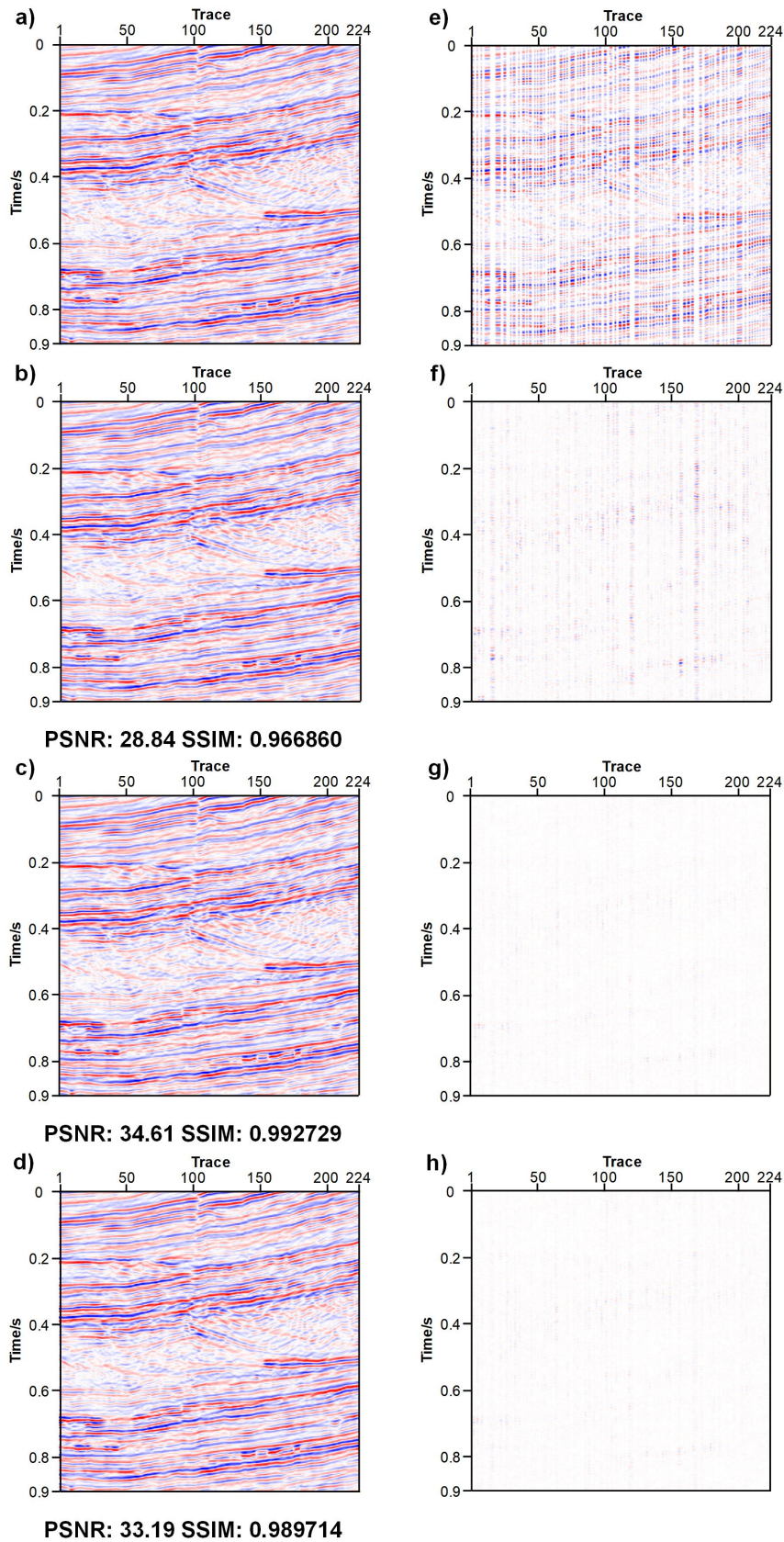


**Figure 8.** Comparisons of the sixth line extracted from Fig. 7. (a) Complete data, (e) 50% randomly sampled data, (b–d) interpolated results of T-2D, T-3D, and T-2.5D, respectively; and (f–h) the corresponding residual images.

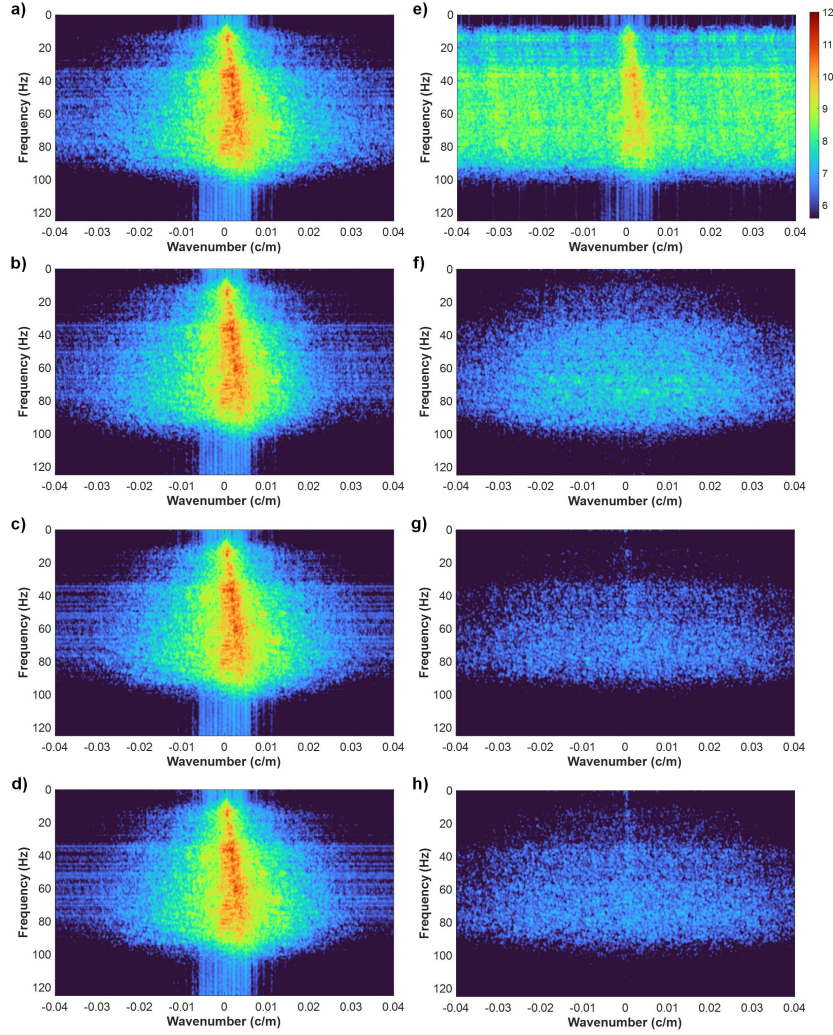


**Figure 9.** (a and e) f-k spectra of the complete data (Fig. 8a) and 50% randomly sampled data (Fig. 8e), (b–d) f-k spectra of the interpolated results by T-2D, T-3D and T2.5D (Fig. 8b–8d), respectively; and (f–h) f-k spectra of the corresponding residual images (Fig. 8f–8h).

achieves comparable interpolation performance to T-3D, while substantially reducing the memory usage and training-time cost, demonstrating that T-2.5D is an efficient DL-based seismic data interpolation method and the proposed cross-dimensional TL is a lightweight process.

**Table 2.** Computational costs of T-2D, T-3D, and T-2.5D on the Kerry dataset.

Method	Peak memory usage (MB)	Training time (h)
T-2D	581	0.46
T-3D	40443	19.90
<b>T-2.5D</b>	<b>3243</b>	<b>0.46 (Stage 1) + 0.65 (Stage 2)</b>

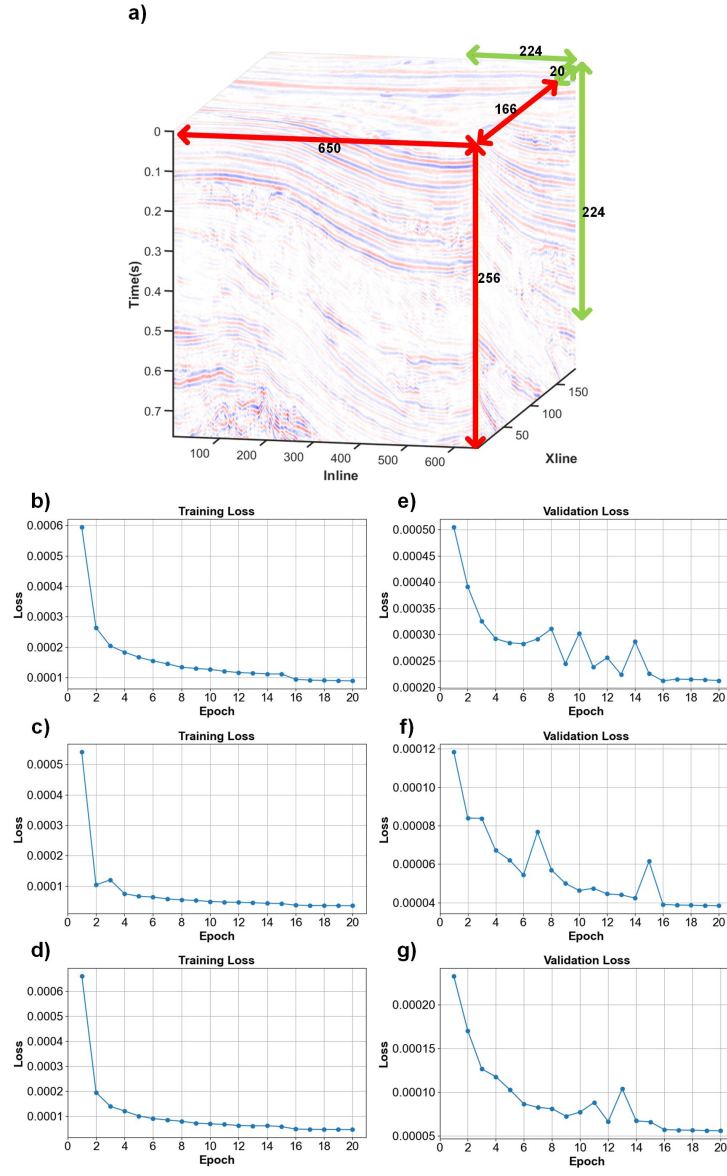


**Figure 10.** (a) 3D Volume of the Parihaka dataset, (b–d) training loss curves of T-2D, T-3D and T-2.5D, respectively; and (e–g) the corresponding validation loss curves.

### 3.4 Test on Parihaka Dataset

#### 3.4.1 Data preparation and training

In this subsection, we use the Parihaka dataset obtained from another survey area of New Zealand to further validate the effectiveness of T-2.5D. As shown in Fig. 10a, the data preparation process of the Parihaka dataset is the same as that of the Kerry dataset. The data preparation of the three methods are given in Table 3. Fig. 10b–10g shows the convergence behavior of the training and validation curves of the three methods on the Parihaka dataset.

**Table 3.** Data preparation of the Parihaka dataset.

Method	Data patch/volume shape	Dataset size	
		Training	Validation
T-2D	40×40	6000	1500
T-3D	40×40×16	6000	1500
<b>T-2.5D</b>	<b>40×40×16</b>	<b>2000 (Stage 2)</b>	<b>500 (Stage 2)</b>

### 3.4.2 Testing results

The 3D data volume ( $224 \times 224 \times 20$ ) defined by green double arrows in Fig. 10a is likewise extracted for testing. As shown in Fig. 11b–11d, the performance of T-2D remains markedly inferior to that of T-3D and T-2.5D, which is also supported by the strongest signal leakage in its residual image (Fig. 11f) and local similarity map (Fig. 11i). In contrast, the performance of T-2.5D is very close to that of T-3D, as shown in Fig. 11h and 11k.

Similarly, the tenth line is illustrated in Fig. 12 as a 2D view. The numerical results in Fig. 12d and little leakage in Fig. 12h indicate the great interpolation ability of T-2.5D.

Fig. 13 displays the f-k spectrum of the complete data (Fig. 12a), 50% randomly sampled data (Fig. 12e), the interpolated results in Fig. 12b–12d, respectively, and the corresponding residual images (Fig. 12f–12h). T-2D still produces more residual interference than the other two methods as indicated by the red arrows and ovals in Fig. 13b. In comparison, the recovered spectrum in Fig. 13d and the energy leakage in Fig. 13h demonstrate the strong interpolation capability of T-2.5D.

### 3.4.3 Analysis of the computational cost

Similar to Kerry dataset, we also provide comparisons of computational cost in Table 4. Due to the same settings of dataset preparation and training, the values on the Parihaka dataset are very similar to that of Kerry dataset. The T-2.5D has achieved great performance at very low computational cost, offering a good trade-off between the effectiveness and efficiency.

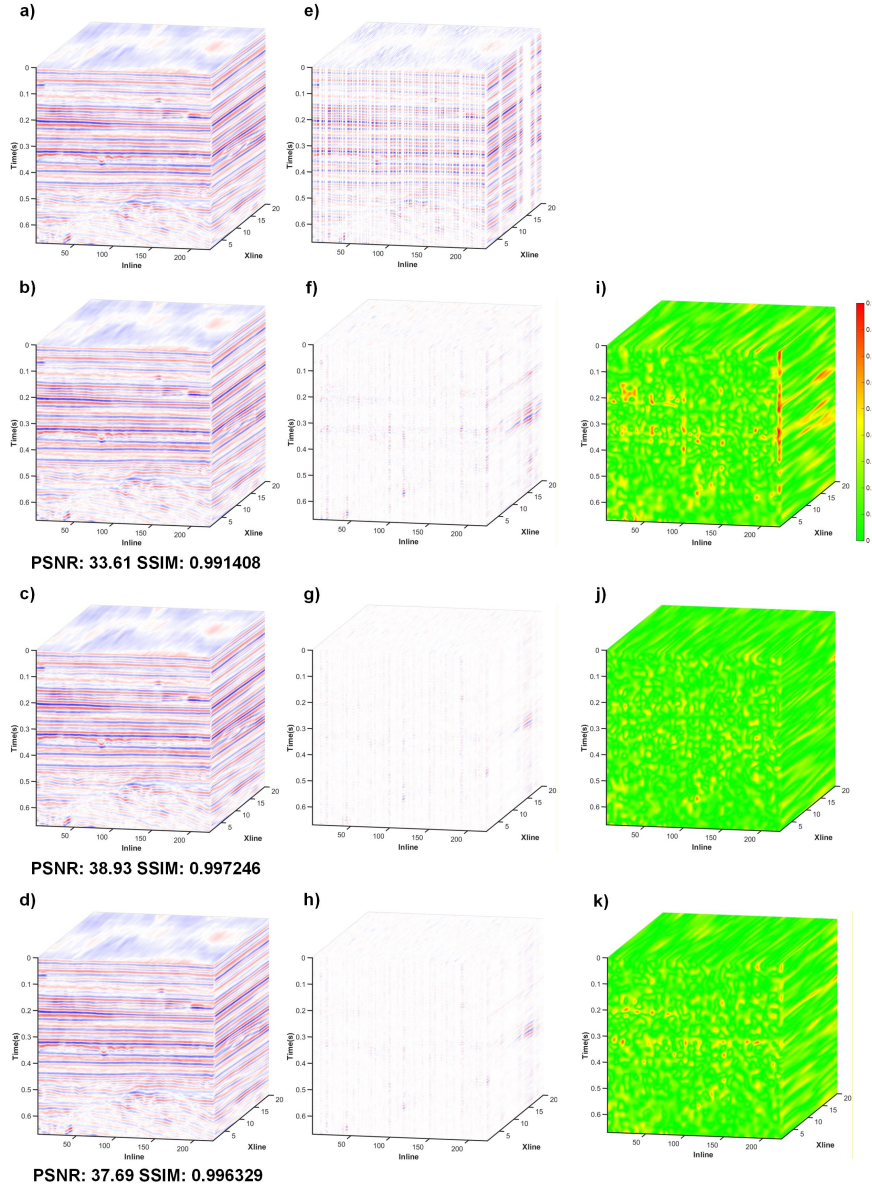


**Figure 11.** Interpolation results of Parihaka dataset. (a) Complete data, (e) 50% randomly sampled data, (b–d) interpolated results of T-2D, T-3D and T-2.5D, respectively; (f–h) the corresponding residual images, and (i–k) local similarity maps between (f–h) and (a).

**Table 4.** Computational costs of T-2D, T-3D, and T-2.5D on the Parihaka dataset.

Method	Peak memory usage (MB)	Training time (h)
T-2D	581	0.44
T-3D	40443	19.94
<b>T-2.5D</b>	<b>3243</b>	<b>0.44 (Stage 1) + 0.65 (Stage 2)</b>

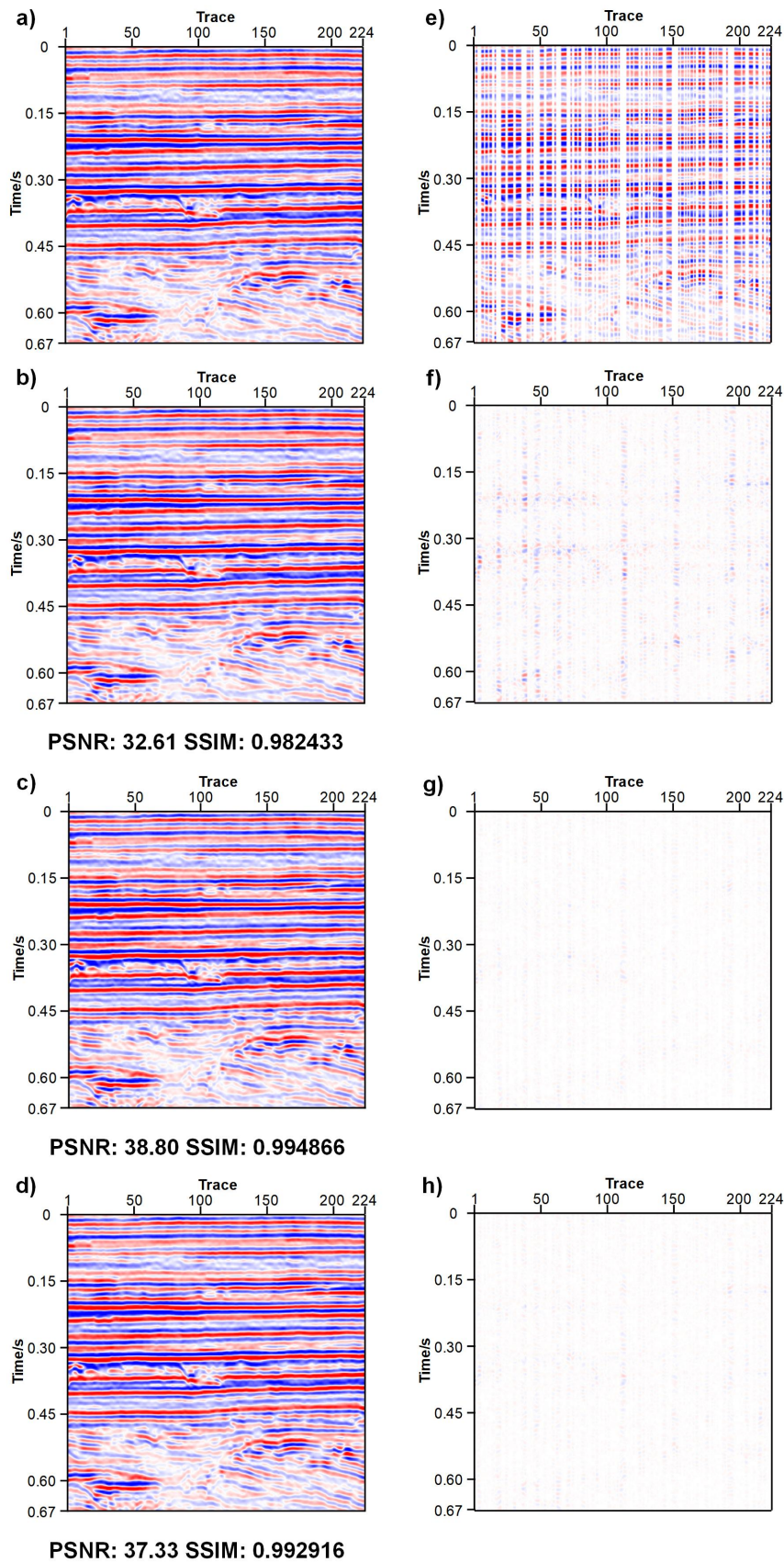


**Figure 12.** Comparisons of the tenth line extracted from Fig. 11. a) Complete data, (e) 50% randomly sampled data, (b–d) interpolated results of T-2D, T-3D, and T-2.5D, respectively; and (f–h) the corresponding residual images.

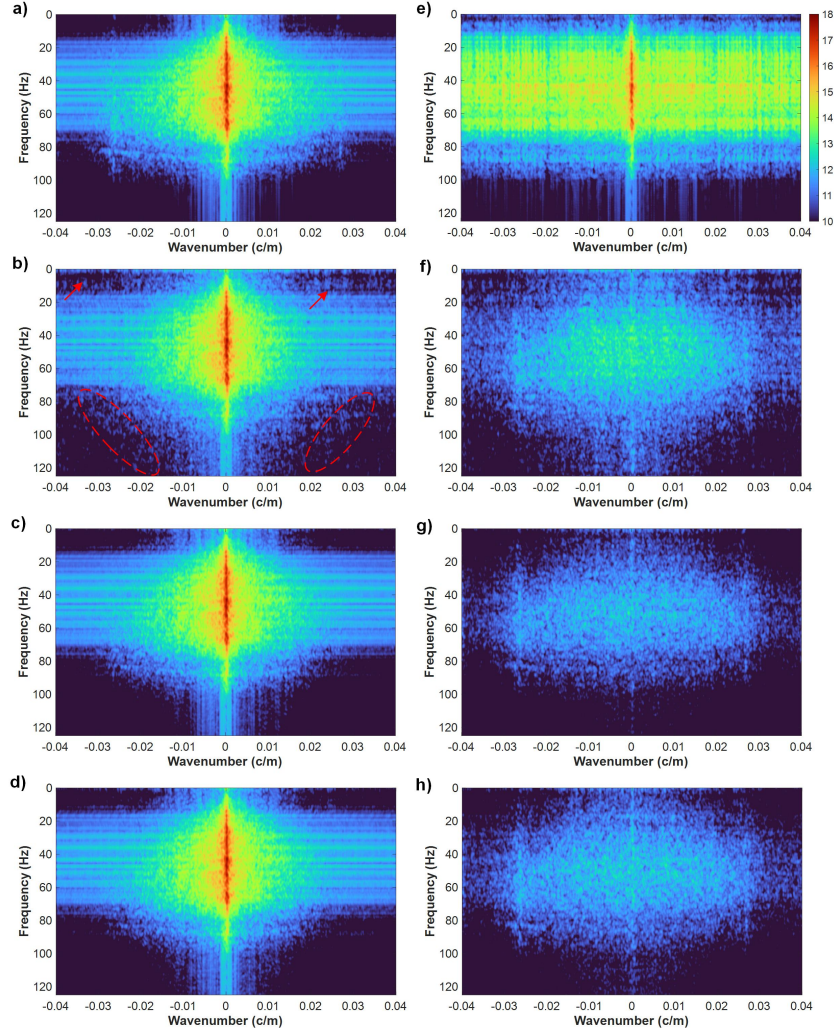


**Figure 13.** (a and e) f-k spectra of the complete data (Fig. 12a) and 50% randomly sampled data (Fig. 12e), (b–d) f-k spectra of the interpolated results by T-2D, T-3D and T2.5D (Fig. 12b–12d), respectively; and (f–h) f-k spectra of the corresponding residual images (Fig. 12f–12h).

### 3.5 Analysis of the computational cost

Generalization is an important ability that allows a DL model to effectively process variant datasets that are not used during training (Zhang et al. 2021). To further explore the generalization capability, the Opunake dataset, which is from another 3D survey in New Zealand, is utilized for further TL of T-2.5D and T-3D. Specifically, we extract approximately 1000 and 250 volumes with a shape of  $40 \times 40 \times 16$  from the full Opunake dataset for training and validation, respectively, and extract a volume with a shape of  $224 \times 224 \times 20$  as test data. Here, TL for T-2.5D and T-3D is performed in a full fine-tuning manner. The comparisons of the interpolated results before and after the TL are

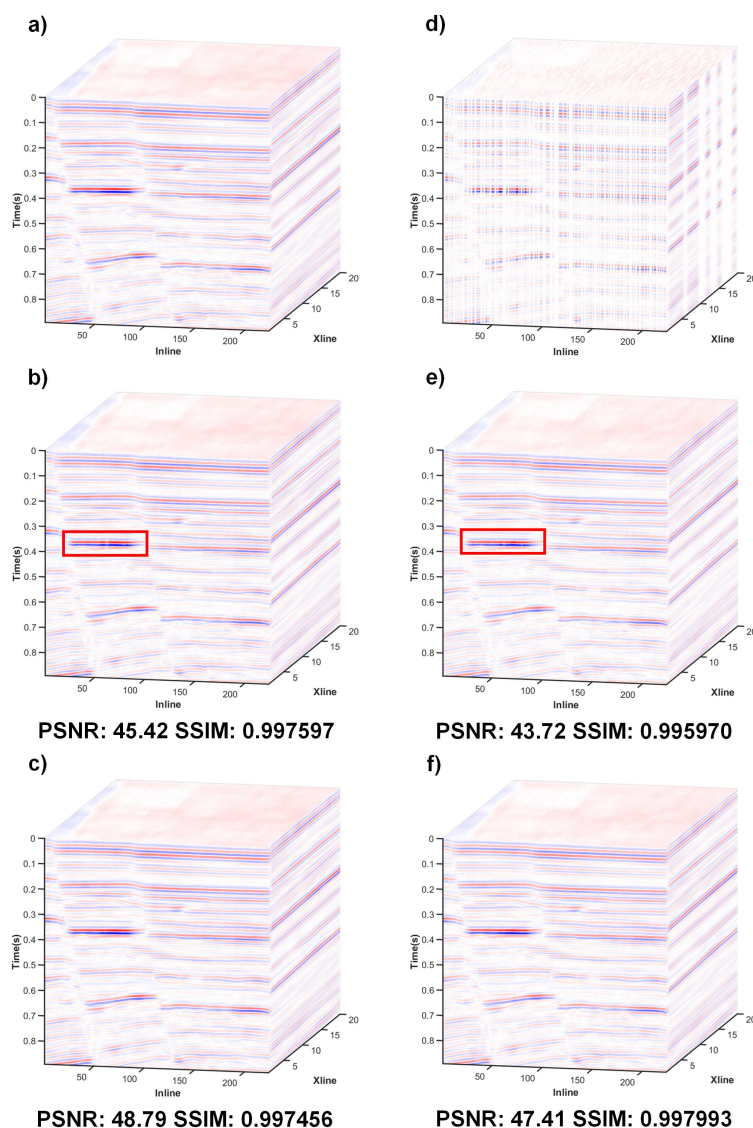


**Figure 14.** Interpolation of randomly sampled data on Opunake dataset. (a) Complete data, (d) 50% randomly sampled data, (b and e) interpolated results of T-3D and T-2.5D before TL, respectively; (c and f) interpolated results of T-3D and T-2.5D after TL, respectively.

presented in Fig. 14. As indicated by the red boxes in Fig. 14b and 14e, the interpolated results before applying TL contain certain discontinuous events. As illustrated in Fig. 14c and 14f, this issue is alleviated after applying TL. The numerical results have also been evidently improved. Meanwhile, Fig. 15 gives the corresponding residual images and local similarity maps. Compared to Fig. 15a, 15e, 15b, 15f, the lower energy in Fig. 15c, 15g, 15d, 15h indicates better interpolation performance after applying TL.

We plot the 20th line of the test data from Fig. 14 for 2D comparison. As shown in Fig. 16b

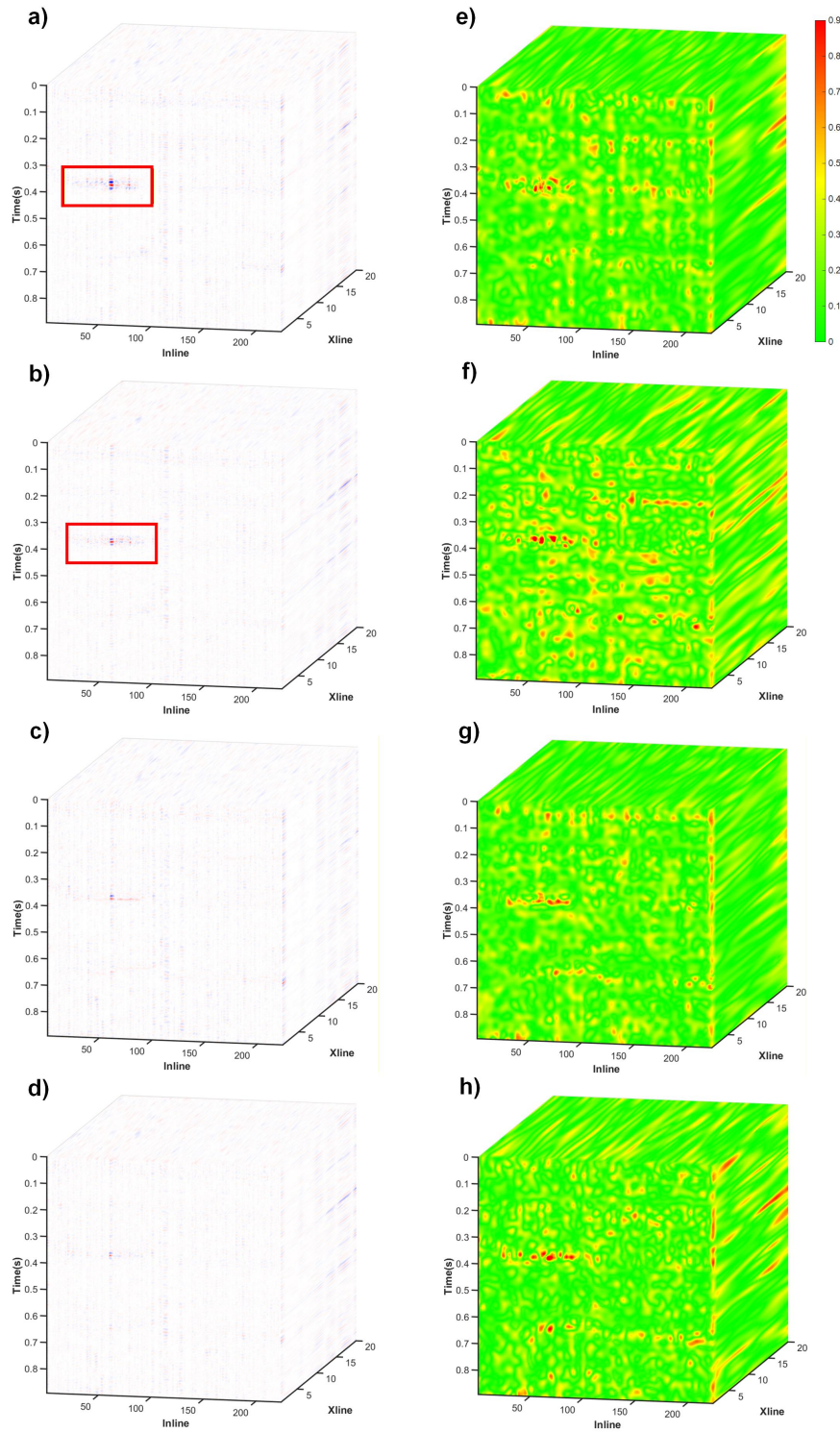


**Figure 15.** (a–d) Residual images of Fig. 14b, 14e, 14c, 14f, respectively, and (e–h) local similarity maps between (a–d) and Fig. 14b, 14e, 14c, 14f, respectively.

and 16c, the two interpolated results before applying TL contain discontinuous events as indicated by the red boxes. After applying TL, the continuity and smoothness have been improved, as shown in Fig. 16d and 16e. T-2.5D still achieves comparable performance to that of T-3D, with an even higher SSIM value. In summary, T-2.5D has great potential for effectively interpolating randomly missing traces in 3D seismic data from different survey areas, exhibiting great generalization ability.

## 4 DISCUSSIONS

### 4.1 Testing in the Regularly Missing Case

All the interpolated results in the previous section are dealing with irregularly missing traces. In fact, T-2.5D can also be leveraged to handle regular gaps to increase the acquisition density. To validate this, we further assess the proposed T-2.5D on the Kerry dataset with 67% regularly missing traces (removing two out of every three traces) in Fig. 17e. As shown in Fig. 17b–17d, the interpolation result of T-2.5D shows superior performance to T-2D. Furthermore, it has achieved even better numerical results than T-3D does under such a high missing rate. The residual image in Fig. 17h further demonstrates that T-2.5D can effectively recover signals with little leakage in the regularly missing scenario.

### 4.2 Comparison of Trainable Parameters

The number of trainable parameters in a network model is also an important factor for DL-based methods. Models with more trainable parameters can represent more complex functions, but may require more memory and computation (Tu et al. 2024). We further compare the trainable parameters of the three networks. Notably, the total trainable parameters of T-2.5D are composed of two parts: the ones from the four Transformer encoders in the first stage, and the ones from the remainder of T-2.5D in the second stage. As shown in Table 5, the trainable parameters surge from 2D to 3D. Although T-2D has the fewest trainable parameters, its interpolation performance is also inferior to the other two networks. Although the total trainable parameters of T-2.5D are only 75.34%

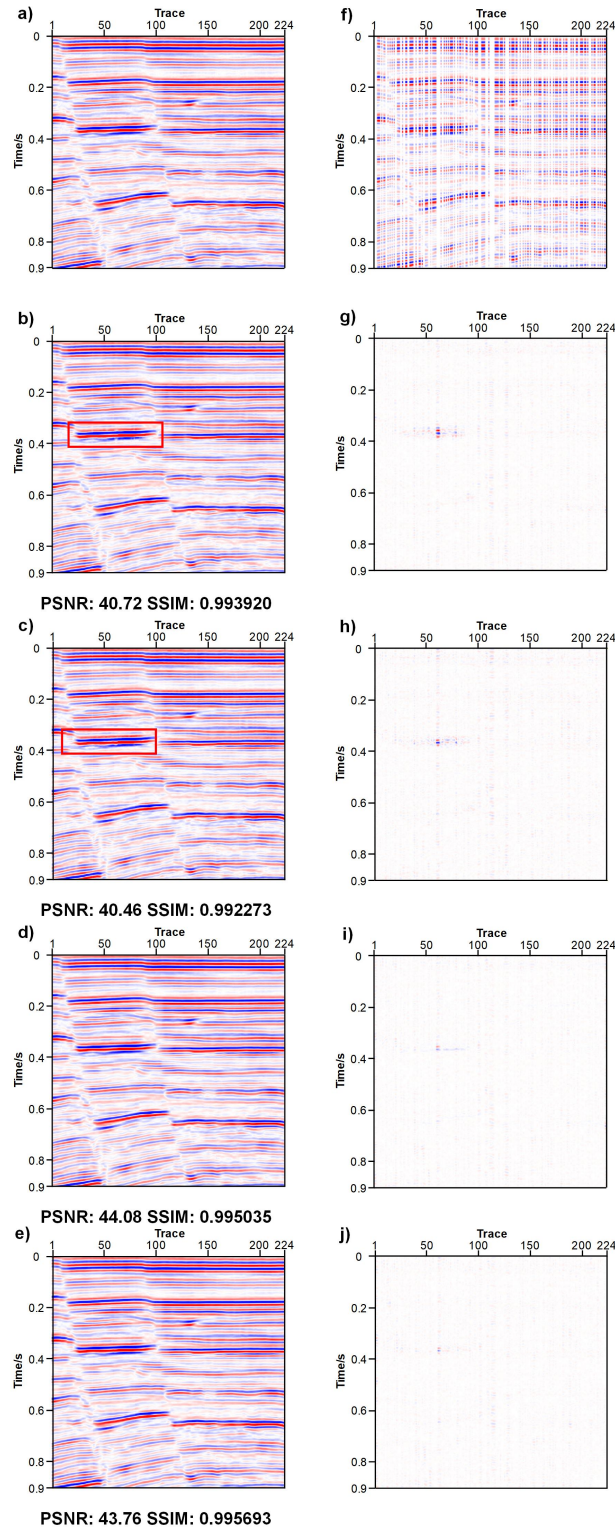


**Figure 16.** Comparisons of the 20th extracted from the Fig. 14. (a) Complete data, (f) 50% randomly sampled data, (b–e) interpolated results of T-3D and T-2.5D before and after applying TL, respectively; and (g–j) the corresponding residual images.

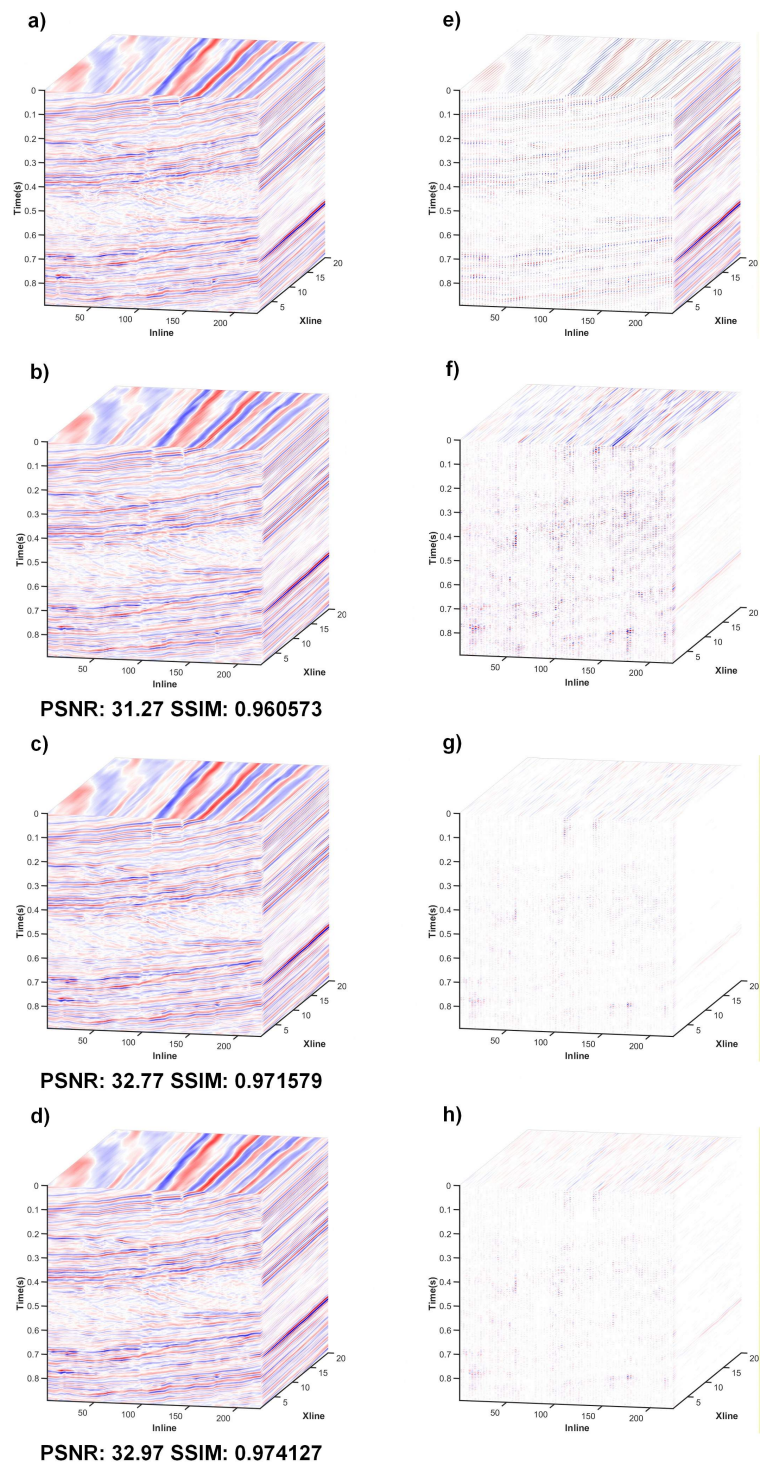


**Figure 17.** Interpolation of regularly sampled data on Kerry dataset. (a) Complete data, (e) 67% regularly sampled data, (b–d) interpolated results of T-2D, T-3D, and T-2.5D, respectively; (f–h) the corresponding residual images.

**Table 5.** Trainable parameters in different networks.

Method	Trainable parameters
T-2D	212289
T-3D	1795953
<b>T-2.5D</b>	<b>34048 (Stage 1) + 1319121 (Stage 2)</b>

of those of T-3D, T-2.5D can achieve performance comparable to T-3D, or even surpassing it in certain cases. This finding further supports the lightweight and efficient nature of T-2.5D.

### 4.3 Comparisons of inference time

In DL-based seismic data pre-processing, the inference time also plays an important role due to the need for processing massive datasets. Hence, we have recorded the inference time of T-2D, T-3D and T-2.5D in randomly missing cases. As shown in Table 6, the inference time of T-2.5D is even less than that of T-2D. This is because T-2D requires additional processing time for splitting and reassembling the 3D volumes, which is not needed in T-2.5D. Meanwhile, it only requires less than 1/9 the inference time of T-3D. These comparisons demonstrate that T-2.5D is capable of interpolating seismic data rapidly with high quality when faced with large-scale 3D seismic datasets.

## 5 CONCLUSION

In this paper, we propose a Transformer-based network, named T-2.5D, to accomplish 3D seismic data interpolation tasks. Specifically, a cross-dimensional TL training strategy is utilized to optimize T-2.5D, so as to reduce the computational burdens when interpolating 3D seismic data

**Table 6.** Inference time of T-2D, T-3D, and T-2.5D.

Method	Inference time (s)		
	Kerry dataset	Parihaka dataset	Opunake Dataset
T-2D	8.29	8.31	N/A
T-3D	66.23	66.12	66.04
<b>T-2.5D</b>	<b>7.14</b>	<b>7.04</b>	<b>7.07</b>

with Transformer. This strategy consists of two stages. The first stage is the 2D pre-training stage. It generates a pre-trained model by optimizing the Transformer encoders in T-2.5D using a large amount of 2D data patches. The second stage is the 3D fine-tuning stage, in which the 3D SDAs are fine-tuned using a small number of 3D data volumes. In this stage, the SDAs, each placed before a Transformer encoder, can learn abundant spatial correlation information across seismic lines. Extensive experiments demonstrate that the T-2.5D with this cross-dimensional strategy exhibits comparable or even better performance to T-3D, while requiring only small amounts of memory and training time. In summary, the proposed T-2.5D is qualified to replace time-consuming, memory-intensive full 3D training, so as to significantly improve the efficiency of 3D interpolation using Transformer.

## ACKNOWLEDGMENTS

This work was jointly supported by the Deep Earth Probe and Mineral Resources Exploration–National Science and Technology Major Project under Grant 2025ZD1007603, and National Natural Science Foundation of China under Grant 42574169.

## 6 DATA AVAILABILITY STATEMENT

The data used in this paper is available at [https://wiki.seg.org/wiki/Open\\_data](https://wiki.seg.org/wiki/Open_data). The implementation details of the algorithm are subject to pending intellectual property protection. Therefore, the source code cannot be openly distributed at this stage. Researchers interested in technical discussions may contact the authors for further clarification.

## REFERENCES

- Cadzow, J. A., 2002. Signal enhancement—a composite property mapping algorithm, *IEEE Transactions on acoustics, speech, and signal processing*, **36**(1), 49–62.
- Cai, J.-F., Ji, H., Shen, Z., & Ye, G.-B., 2014. Data-driven tight frame construction and image denoising, *Applied and Computational Harmonic Analysis*, **37**(1), 89–105.
- Carozzi, F. & Sacchi, M. D., 2021. Interpolated multichannel singular spectrum analysis: A reconstruction method that honors true trace coordinates, *Geophysics*, **86**(1), V55–V70.

- Chen, G., Liu, Y., Zhang, M., Sun, Y., & Zhang, H., 2024. Low-rank approximation reconstruction of five-dimensional seismic data, *Surveys in Geophysics*, **45**(5), 1459–1492.
- Chen, Y., Chen, X., Wang, Y., & Zu, S., 2019. The interpolation of sparse geophysical data, *Surveys in Geophysics*, **40**(1), 73–105.
- Chen, Y., Yu, S., & Ma, J., 2023. A projection-onto-convex-sets network for 3d seismic data interpolation, *Geophysics*, **88**(3), V249–V265.
- Cheng, M., Lin, J., Lu, S., Dong, S., & Dong, X., 2023. Seismic data reconstruction based on multiscale attention deep learning, *IEEE Transactions on Geoscience and Remote Sensing*, **61**, 1–18.
- Cheng, M., Lin, J., Dong, X., Lu, S., & Zhong, T., 2024a. Seismic interpolation transformer for consecutively missing data: A case study in das-vsp data, *IEEE Transactions on Geoscience and Remote Sensing*.
- Cheng, S., Harsuko, R., & Alkhalifah, T., 2024b. Meta-processing: A robust framework for multi-tasks seismic processing, *Surveys in Geophysics*, **45**(4), 1081–1116.
- Cheng, S., Harsuko, R., & Alkhalifah, T., 2025. A generative foundation model for an all-in-one seismic processing framework, *Surveys in Geophysics*.
- Dong, X., Lin, J., Lu, S., Huang, X., Wang, H., & Li, Y., 2022. Seismic shot gather denoising by using a supervised-deep-learning method with weak dependence on real noise data: A solution to the lack of real noise data, *Surveys in Geophysics*, **43**(5), 1363–1394.
- Dong, X., Lu, S., Lin, J., Zhang, S., Ren, K., & Cheng, M., 2024a. Can deep learning compensate for sparse shots in the imaging domain? a potential alternative for reducing the acquisition cost of seismic data, *Geophysics*, **89**(2), V119–V137.
- Dong, X., Wei, C., Zhong, T., Cheng, M., Dong, S., & Li, F., 2024b. Seismic data reconstruction based on a multicascade self-guided network, *Geophysics*, **89**(3), V179–V195.
- Dong, X., Wei, C., Lin, J., Lu, S., Cheng, M., & Zhang, R., 2025. Deep-learning-based global feature capture for seismic data reconstruction, *Geophysics*, **90**(5), V499–V511.
- Dosovitskiy, A., 2020. An image is worth 16x16 words: Transformers for image recognition at scale, *arXiv preprint arXiv:2010.11929*.
- Fang, W., Fu, L., Zhang, M., & Li, Z., 2021. Seismic data interpolation based on u-net with texture loss, *Geophysics*, **86**(1), V41–V54.
- Fomel, S., 2003. Seismic reflection data interpolation with differential offset and shot continuation, *Geophysics*, **68**(2), 733–744.
- Fomel, S., 2007. Local seismic attributes, *Geophysics*, **72**(3), A29–A33.
- Fomel, S. & Liu, Y., 2010. Seislet transform and seislet frame, *Geophysics*, **75**(3), V25–V38.
- Gao, J., Sacchi, M. D., & Chen, X., 2013. A fast reduced-rank interpolation method for prestack seismic volumes that depend on four spatial dimensions, *Geophysics*, **78**(1), V21–V30.

- Gao, L., Shen, H., & Min, F., 2024. Swin transformer for simultaneous denoising and interpolation of seismic data, *Computers & Geosciences*, **183**, 105510.
- Goodfellow, I. J., Pouget-Abadie, J., Mirza, M., Xu, B., Warde-Farley, D., Ozair, S., Courville, A., & Bengio, Y., 2014. Generative adversarial nets, in *Advances in Neural Information Processing Systems*, vol. 27, Curran Associates, Inc.
- He, K., Zhang, X., Ren, S., & Sun, J., 2016. Deep residual learning for image recognition, in *Proceedings of the IEEE Conference on Computer Vision and Pattern Recognition (CVPR)*.
- Huang, G., Liu, Z., van der Maaten, L., & Weinberger, K. Q., 2017. Densely connected convolutional networks, in *Proceedings of the IEEE Conference on Computer Vision and Pattern Recognition (CVPR)*.
- Huang, W., Wang, R., Zhou, Y., Chen, Y., & Yang, R., 2016. *Improved principal component analysis for 3D seismic data simultaneous reconstruction and denoising*, pp. 4102–4106.
- Huang, W., Feng, D., & Chen, Y., 2020. De-aliased and de-noise cadzow filtering for seismic data reconstruction, *Geophysical Prospecting*, **68**(2), 553–571.
- Jia, Y. & Ma, J., 2017. What can machine learning do for seismic data processing? an interpolation application, *GEOPHYSICS*, **82**(3), V163–V177.
- Jin, Z., Li, X., Yang, H., Wu, B., & Zhu, X., 2023. Depthwise separable convolution unet for 3d seismic data interpolation, *Frontiers in Earth Science*, **Volume 10 - 2022**.
- Kingma, D. P. & Ba, J., 2014. Adam: A method for stochastic optimization, *arXiv preprint*.
- Kumar, R., Da Silva, C., Akalin, O., Aravkin, A. Y., Mansour, H., Recht, B., & Herrmann, F. J., 2015. Efficient matrix completion for seismic data reconstruction, *Geophysics*, **80**(5), V97–V114.
- LeCun, Y., Bengio, Y., & Hinton, G., 2015. Deep learning, *nature*, **521**(7553), 436–444.
- Liang, J., Ma, J., & Zhang, X., 2014. Seismic data restoration via data-driven tight frame, *Geophysics*, **79**(3), V65–V74.
- Liu, C., Wang, D., Sun, J., & Wang, T., 2018. Crossline-direction reconstruction of multi-component seismic data with shearlet sparsity constraint, *Journal of Geophysics and Engineering*, **15**(5), 1929–1942.
- Liu, N., Wu, L., Wang, J., Wu, H., Gao, J., & Wang, D., 2022a. Seismic data reconstruction via wavelet-based residual deep learning, *IEEE Transactions on Geoscience and Remote Sensing*, **60**, 1–13.
- Liu, Y., Wu, G., & Zheng, Z., 2022b. Seismic data interpolation without iteration using at-x-y streaming prediction filter with varying smoothness, *Geophysics*, **87**(1), V29–V38.
- Ma, J., 2013. Three-dimensional irregular seismic data reconstruction via low-rank matrix completion, *Geophysics*, **78**(5), V181–V192.
- Naghizadeh, M. & Sacchi, M., 2013. Multidimensional de-aliased cadzow reconstruction of seismic records, *Geophysics*, **78**(1), A1–A5.
- Naghizadeh, M. & Sacchi, M. D., 2007. Multistep autoregressive reconstruction of seismic records, *Geophysics*, **72**(6), V111–V118.

- Naghizadeh, M. & Sacchi, M. D., 2010. Beyond alias hierarchical scale curvelet interpolation of regularly and irregularly sampled seismic data, *Geophysics*, **75**(6), WB189–WB202.
- Oliveira, D. A., Ferreira, R. S., Silva, R., & Brazil, E. V., 2018. Interpolating seismic data with conditional generative adversarial networks, *IEEE Geoscience and Remote Sensing Letters*, **15**(12), 1952–1956.
- Oropeza, V. & Sacchi, M., 2011. Simultaneous seismic data denoising and reconstruction via multichannel singular spectrum analysis, *Geophysics*, **76**(3), V25–V32.
- Pan, J., Lin, Z., Zhu, X., Shao, J., & Li, H., 2022. St-adapter: Parameter-efficient image-to-video transfer learning, in *Advances in Neural Information Processing Systems*, vol. 35, pp. 26462–26477, Curran Associates, Inc.
- Park, J., Yoon, D., Seol, S. J., & Byun, J., 2019. Reconstruction of seismic field data with convolutional u-net considering the optimal training input data, in *SEG International Exposition and Annual Meeting*, p. D023S027R005.
- Park, J., Choi, J., Jee Seol, S., Byun, J., & Kim, Y., 2021. A method for adequate selection of training data sets to reconstruct seismic data using a convolutional u-net, *Geophysics*, **86**(5), V375–V388.
- Qian, F., Liu, Z., Wang, Y., Liao, S., Pan, S., & Hu, G., 2021. Dtae: Deep tensor autoencoder for 3-d seismic data interpolation, *IEEE Transactions on Geoscience and Remote Sensing*, **60**, 1–19.
- Ronen, J., 1987. Wave-equation trace interpolation, *Geophysics*, **52**(7), 973–984.
- Ronneberger, O., Fischer, P., & Brox, T., 2015. U-net: Convolutional networks for biomedical image segmentation, in *Medical Image Computing and Computer-Assisted Intervention – MICCAI 2015*, pp. 234–241, Springer International Publishing, Cham.
- Saad, O. M., Fomel, S., Abma, R., & Chen, Y., 2023. Unsupervised deep learning for 3d interpolation of highly incomplete data, *Geophysics*, **88**(1), WA189–WA200.
- Siahkoohi, A., Kumar, R., & Herrmann, F., 2018. Seismic data reconstruction with generative adversarial networks, in *80th EAGE conference and exhibition 2018*, vol. 2018, pp. 1–5, European Association of Geoscientists & Engineers.
- Spitz, S., 1991. Seismic trace interpolation in the fx domain, *Geophysics*, **56**(6), 785–794.
- Trad, D. O., Ulrych, T. J., & Sacchi, M. D., 2002. Accurate interpolation with high-resolution time-variant radon transforms, *Geophysics*, **67**(2), 644–656.
- Trickett, S., Burroughs, L., Milton, A., Walton, L., & Dack, R., 2010. Rank-reduction-based trace interpolation, in *SEG International Exposition and Annual Meeting*, pp. SEG–2010–3829.
- Tu, X., He, Z., Huang, Y., Zhang, Z.-H., Yang, M., & Zhao, J., 2024. An overview of large ai models and their applications, *Visual Intelligence*, **2**(1), 34.
- Vaswani, A., Shazeer, N., Parmar, N., Uszkoreit, J., Jones, L., Gomez, A. N., Kaiser, L. u., & Polosukhin, I., 2017. Attention is all you need, in *Advances in Neural Information Processing Systems*, vol. 30, Curran Associates, Inc.

- Vautard, R. & Ghil, M., 1989. Singular spectrum analysis in nonlinear dynamics, with applications to paleoclimatic time series, *Physica D: Nonlinear Phenomena*, **35**(3), 395–424.
- Vyas, A., Katharopoulos, A., & Fleuret, F., 2020. Fast transformers with clustered attention, in *Advances in Neural Information Processing Systems*, vol. 33, pp. 21665–21674, Curran Associates, Inc.
- Wang, B., Zhang, N., Lu, W., Zhang, P., & Geng, J., 2018. Seismic data interpolation using deep learning based residual networks, in *80th EAGE Conference and Exhibition 2018*, vol. 2018, pp. 1–5, European Association of Geoscientists & Engineers.
- Wang, B., Zhang, N., Lu, W., & Wang, J., 2019. Deep-learning-based seismic data interpolation: A preliminary result, *Geophysics*, **84**(1), V11–V20.
- Wang, H., Chen, W., Zhang, Q., Liu, X., Zu, S., & Chen, Y., 2020. Fast dictionary learning for high-dimensional seismic reconstruction, *IEEE Transactions on Geoscience and Remote Sensing*, **59**(8), 7098–7108.
- Wang, X., Ge, Q., Dong, X., Dong, S., & Zhong, T., 2025. Self-supervised diffusion model for 3d seismic data reconstruction, *Geophysics*, **90**(5), 1–124.
- Wang, Z., Bovik, A. C., Sheikh, H. R., & Simoncelli, E. P., 2004. Image quality assessment: from error visibility to structural similarity, *IEEE transactions on image processing*, **13**(4), 600–612.
- Wold, S., Esbensen, K., & Geladi, P., 1987. Principal component analysis, *Chemometrics and Intelligent Laboratory Systems*, **2**(1), 37–52, Proceedings of the Multivariate Statistical Workshop for Geologists and Geochemists.
- Wu, S., Wang, B., Zhao, L., Liu, H., & Geng, J., 2023. High-efficiency and high-precision seismic trace interpolation for irregularly spatial sampled data by combining an extreme gradient boosting decision tree and principal component analysis, *Geophysical Prospecting*, **72**(1 Machine learning applications in geophysical exploration and monitoring), 229–246.
- Yang, Y., Ma, J., Osher, S., et al., 2013. Seismic data reconstruction via matrix completion, *Inverse Problems and Imaging*, **7**(4), 1379–1392.
- Ye, R., Liu, F., & Zhang, L., 2019. 3d depthwise convolution: Reducing model parameters in 3d vision tasks, in *Advances in Artificial Intelligence*, pp. 186–199, Springer International Publishing, Cham.
- Yu, J. & Wu, B., 2021. Attention and hybrid loss guided deep learning for consecutively missing seismic data reconstruction, *IEEE Transactions on Geoscience and Remote Sensing*, **60**, 1–8.
- Yu, S., Ma, J., Zhang, X., & Sacchi, M. D., 2015. Interpolation and denoising of high-dimensional seismic data by learning a tight frame, *Geophysics*, **80**(5), V119–V132.
- Yu, Z., Ferguson, J., McMechan, G., & Anno, P., 2007. Wavelet-radon domain dealiasing and interpolation of seismic data, *Geophysics*, **72**(2), V41–V49.
- Zhang, C., Bengio, S., Hardt, M., Recht, B., & Vinyals, O., 2021. Understanding deep learning (still) requires rethinking generalization, *Commun. ACM*, **64**(3), 107–115.